

Photoinduced magnetism and long-range ordering in rubidium cobalt hexacyanoferrate Prussian blue analog nanoparticles

Daniel M. Pajerowski and Mark W. Meisel

*Department of Physics and the Center of Condensed Matter Sciences,
University of Florida, Gainesville, FL 32611-8440*

Franz A. Frye and Daniel R. Talham

Department of Chemistry, University of Florida, Gainesville, FL 32611-7200

(Dated: March 5, 2019)

Nanoparticles of rubidium cobalt hexacyanoferrate ($\text{Rb}_j\text{Co}_k[\text{Fe}(\text{CN})_6]_l \cdot n\text{H}_2\text{O}$) were synthesized using different concentrations of the organic ligand polyvinylpyrrolidone (PVP) to produce four different batches of particles with characteristic diameters ranging from nominally 3 to 13 nm. Upon illumination with white light at 5 K, the magnetization of these particles increases. In addition, the magnetic properties, namely the long-range ferrimagnetic ordering temperature (T_c) and the coercive field (H_c), of the nanoparticles evolve with preparation protocol. At 2 K, particles with diameters less than 10 nm are in the superparamagnetic limit.

The investigation of the molecule-based magnetism of Prussian blue, $\text{Fe}_4[\text{Fe}(\text{CN})_6]_3 \cdot x\text{H}_2\text{O}$, and related analogs has a rich history [1, 2], dating back to 1928 [3]. Measurements down to liquid helium temperatures identified the transition to long-range ferromagnetic order [4, 5, 6], but an understanding of the magnetic interactions remained elusive until the 1970s, when X-ray [7] and neutron [8] diffraction data identified the crystal structure and the spin transfer from high-spin Fe(III) to low-spin Fe(II). Interest in these materials was renewed in the 1990s with the synthesis of several mixed-metal Prussian blue analogs with higher magnetic ordering temperatures, along with the 1996 discovery of long-lived, photoinduced magnetism in $\text{K}_{0.2}\text{Co}_{1.4}[\text{Fe}(\text{CN})_6] \cdot 6.9\text{H}_2\text{O}$ [9]. A flurry of experimental and theoretical research has elucidated the fundamental nature of the light-induced effects in three-dimensional bulk materials [10, 11], and recent efforts have been made to integrate the photoinduced magnetism into films [12, 13, 14, 15, 16, 17, 18] and nanoparticles, which have technical and biophysical applications. Numerous efforts to synthesize nanoparticles of Prussian blue analogs have been made, but only a few examples of photoinduced magnetism have been reported, including work that isolated $\text{K}_j\text{Co}_k[\text{Fe}(\text{CN})_6]_l \cdot n\text{H}_2\text{O}$ particles, with typical diameters of 8 – 10 nm, within a silica xerogel [19], and other research producing 11 nm \times 70 nm nanorods of $\text{Mo}(\text{CN})_8\text{Cu}_2$ protected by polyvinylpyrrolidone (PVP) [20]. In each case, although photoinduced magnetism was observed, the particles did not exhibit long-range order.

The purpose of this letter is to report our ability to synthesize $\text{Rb}_j\text{Co}_k[\text{Fe}(\text{CN})_6]_l \cdot n\text{H}_2\text{O}$ nanoparticles, protected by PVP, that exhibit photoinduced magnetism for all sizes and that possess long-range ordering, with coercive fields ranging between 0.25 – 1.5 kG, in the larger particles. From the data, the superparamagnetic limit at 2 K is identified, and the magnetic signal generated from particles in this limit can be estimated for the different

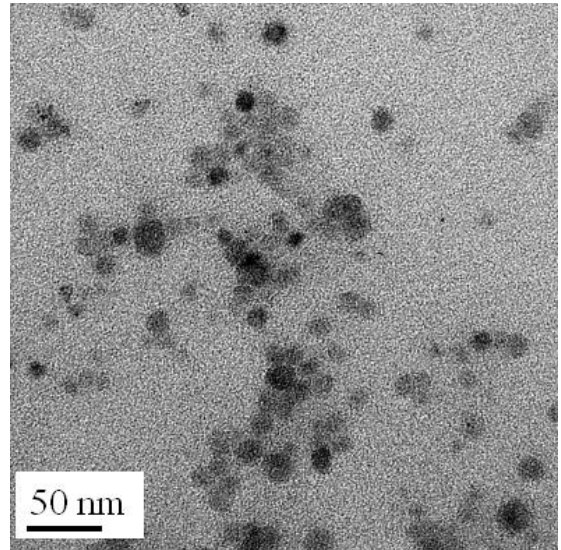


FIG. 1: Typical TEM image of a collection of nanoparticles, and this specific image is from Batch D, see Table 1.

batches of particles.

The nanoparticles were synthesized by modifying the procedure described by Uemura and coworkers [21, 22]. A 2 mL solution containing both 28 mg $\text{K}_3\text{Fe}(\text{CN})_6$ (0.085 mM) and 6.8 mg RbNO_3 (0.046 mM) was added dropwise to an 8 mL solution containing 30 mg $\text{Co}(\text{NO}_3)_2 \cdot 6\text{H}_2\text{O}$ (0.103 mM) and PVP while stirring rapidly. By varying the amount of PVP (Table 1), the protocol produced samples with different particle sizes and size distributions. After 30 minutes of stirring, the solution was allowed to sit for one week. For the transmission electron microscopy (TEM) studies, a 50 μL aliquot of the suspension was diluted 2000 times, and 8 μL of the diluted suspension was placed on a holey carbon grid. A representative image is shown in Fig. 1,

TABLE I: A summary of the materials properties of the four sets of samples.

Batch	Starting PVP (g)	Resulting chemical formula	PVP:Co ratio	Diameter (nm)	$T_{c,onset}^{\text{dark}}$ (K)	$T_{c,onset}^{\text{light}}$ (K)	H_c^{dark} (G)	H_c^{light} (G)
A	1.0	$\text{Rb}_{1.9}\text{Co}_4(\text{Fe}(\text{CN})_6)_{3.2} \cdot (\text{H}_2\text{O})_{4.8}$	360	3.3 ± 0.8	< 2	< 2	< 10	< 10
B	0.5	$\text{Rb}_{1.8}\text{Co}_4(\text{Fe}(\text{CN})_6)_{3.2} \cdot (\text{H}_2\text{O})_{4.8}$	200	6.9 ± 2.5	10	13	~ 15	~ 30
C	0.2	$\text{Rb}_{1.7}\text{Co}_4(\text{Fe}(\text{CN})_6)_{3.2} \cdot (\text{H}_2\text{O})_{4.8}$	60	9.7 ± 2.1	13	17	250	330
D	0.1	$\text{Rb}_{0.9}\text{Co}_4(\text{Fe}(\text{CN})_6)_{2.9} \cdot (\text{H}_2\text{O})_{6.6}$	20	13.0 ± 3.2	19	22	1000	1500

and selected area electron diffraction was compared to powder X-ray diffraction patterns to confirm the structure [23]. In addition, infrared spectra displayed a C-N stretch of 2124 cm^{-1} consistent with a Co(III)-Fe(II) low spin pair. Using Image J imaging software [24], the TEM images were analyzed to obtain the particle size distributions shown in Fig. 2 [25]. These data were fit to a log-normal function that yielded the characteristic diameters shown in Fig. 2 and Table 1. To isolate the particles, three volumes of acetone were added to the synthesis solution, which was centrifuged, and then further washed with acetone and dried under vacuum. Chemical analysis was obtained from a combination of CHN combustion analysis and inductively coupled plasma mass spectroscopy (ICP-MS), and the resulting formula are listed in Table 1, along with the ratio of the PVP repeat unit per cobalt. The concentration of H_2O coordinated to the Co was estimated by considering the Fe vacancies.

The temperature dependences of the dc magnetic susceptibilities, $\chi(T)$, of the four batches of particles are shown in Fig. 3. A standard commercial SQUID magnetometer was employed, and the samples were mounted to commercial transparent tape and could be irradiated with light from a room-temperature, halogen source by using a homemade probe equipped with a bundle of optical fibers [17]. Background contributions from the holder and tape have been independently measured and have been subtracted from the data. The magnetic signals are expressed per mole of Prussian blue analog (PBA), Table 1. The dark state ZFC data were obtained after cooling in zero applied field from 300 K, while the dark state FC data were taken after cooling in 100 G from 300 K. The light state was established after field cooling the samples from 300 K to 5 K in 100 G and subsequently irradiating with light for 5 hours. The light state FC data were obtained after cooling from 30 K in 100 G.

It is noteworthy to recall that the photoinduced magnetic properties of the Prussian blue analogs depends upon a charge transfer and spin crossover effect, while the presence of vacancies allow crystalline flexibility [26, 27, 28, 29, 30, 31, 32, 33]. More specifically for $\text{Rb}_j\text{Co}_k[\text{Fe}(\text{CN})_6]_l \cdot n\text{H}_2\text{O}$, the spins can exist in either of two arrangements. The low-spin state consists of Fe(II) ($S = 0$) and Co(III) ($S = 0$), while the high-spin state possesses Fe(III) ($S = 1/2$) and Co(II) ($S = 3/2$). De-

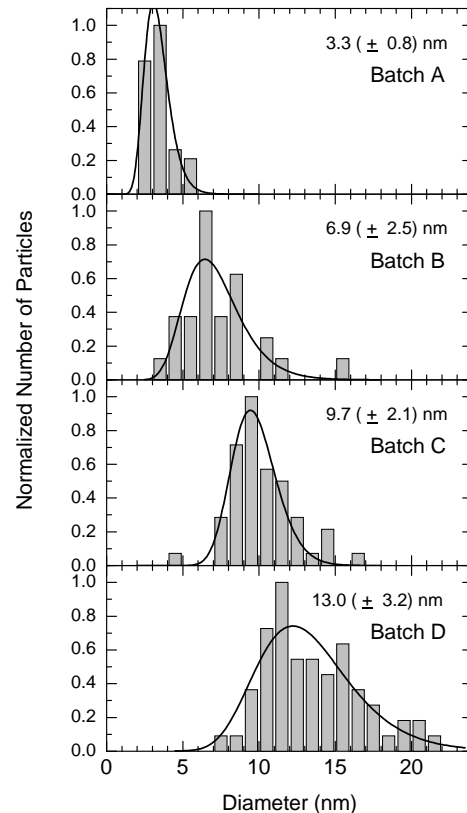


FIG. 2: The particle distributions, normalized to the largest bin, versus diameter for the four batches of particles, see Table 1. The total number of particles for each distribution, smallest to largest, is 44, 27, 53, and 62, respectively. The solid lines are the results of log-normal fits that provide the characteristic diameters shown for each distribution.

pending on the local chemical environment due to the values of j , k , l , and n in the chemical formula, the Fe and Co spins can be locked into either their high-spin or low-spin states for all accessible temperatures. Alternatively, with the proper tuning of the chemical ratios, the Fe and Co ions can exist in high-spin states at room temperature and then experience a crossover to their low-spin states at approximately 150 K. The spin crossover phenomenon generates the photoswitchable pairs involved in the photoinduced magnetism. However, since the spin crossover effect may not be 100% efficient, some regions remain

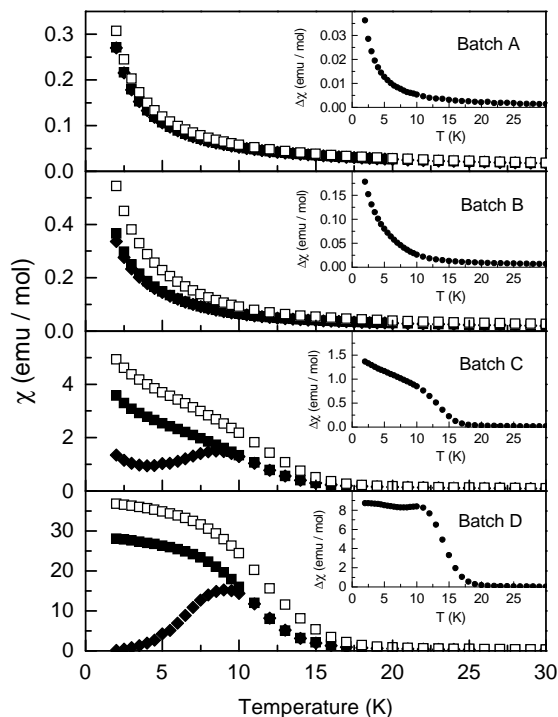


FIG. 3: The temperature dependences of the low field, 100 G, susceptibilities are shown for the zero-field cooled (ZFC) dark (\blacklozenge), field-cooled (FC) dark (\blacksquare), and FC light (\square) states of each batch produced. The insets display the differences between the FC light and dark states, as described in the text. Finite values for this difference can only arise from photoinduced magnetism.

locked in their high-spin states, and we refer to them as primordial spins [13]. For example, these primordial spins are responsible for the magnetic signals observed for the dark state of the largest particles. When irradiated, the low-spin regions, near the primordial high-spin clusters, are photoinduced to the high-spin magnetic state, resulting in a growth of the magnetic domain. This scenario is supported by our description of the anisotropic photoinduced magnetism observed in films [13, 18], by our frequency dependent ac susceptibility studies [34], and by the local probe investigations of others [35, 36].

All samples reported show a photoinduced increase in their magnetic signals, and the strength of the change is correlated with the size of the particles. The differences between the FC susceptibilities of the light and dark states, $\Delta\chi = \chi_{\text{FC}}^{\text{light}} - \chi_{\text{FC}}^{\text{dark}}$, are plotted in the insets of Fig. 3, and finite values can only arise from the photoinduced magnetism.

Two main features are seen when considering the evolution of material properties due to the increasing average size of the separate batches, namely the onset of long-range magnetic order and an increasing net magnetization. This scaling of magnetization is linked to

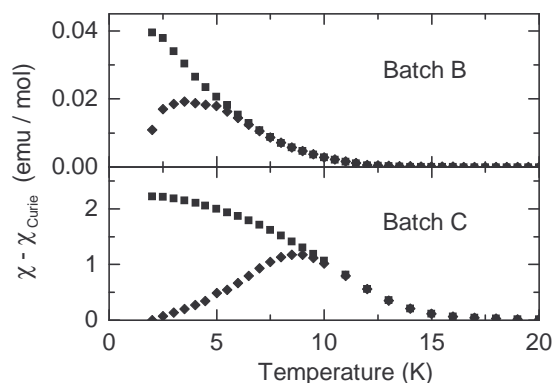


FIG. 4: The primordial ZFC (\blacklozenge) and FC (\blacksquare) states show a signal associated with long-range order for the two batches displaying a mix of magnetic behavior after subtracting the Curie-like contribution.

an increased diamagnetic-surface to magnetically-active-volume ratio at smaller particle sizes. At low temperatures, the high-spin Fe and Co ions interact antiferromagnetically, giving rise to a ferrimagnetic transition at T_c , which is about 24 K for bulk powder specimens with a similar chemical formula [28]. For the magnetic data shown in Fig. 3, the onset of this transition can be estimated, and these macroscopic temperatures are listed in Table 1. We contend that particles larger than a critical size will allow domains large enough to approach bulk-like magnetic properties. Conversely, smaller particles may put limits on allowed domain size, suppressing the ordering temperature. Microscopically, if the size of the magnetic domains is less than or of the order of the magnetic coherence length, then a spectrum of T_c values can be expected until the superparamagnetic limit is achieved.

Consider the magnetic properties of the samples presented in conjunction with the TEM analysis. Batch A has no observed coercivity and follows Curie-like behavior. Batches B and C show a combination of Curie-tail and partial ordering with a reduced T_c (Figs. 3 and 4), as well as finite coercive fields. Finally, the active sites in Batch D are almost entirely ferrimagnetically ordered with the largest coercive field of all batches presented. In addition, the differences between the FC and ZFC data for the dark state in Batch D is consistent with spin glass or cluster glass behavior [34, 37, 38], in accord with the presence of large magnetic domains. In other words, analysis of the data suggests that the superparamagnetic contribution for each of the four batches of nanoparticles (smallest to largest) is 100%, 90%, 50%, and 10%. Consequently, at least down to 2 K, nanoparticles with sizes below ~ 10 nm are in the superparamagnetic limit. These interpretations are consistent with our M versus H measurements performed at 2 K, where coercive fields, H_c , and remnant magnetization values are observed for

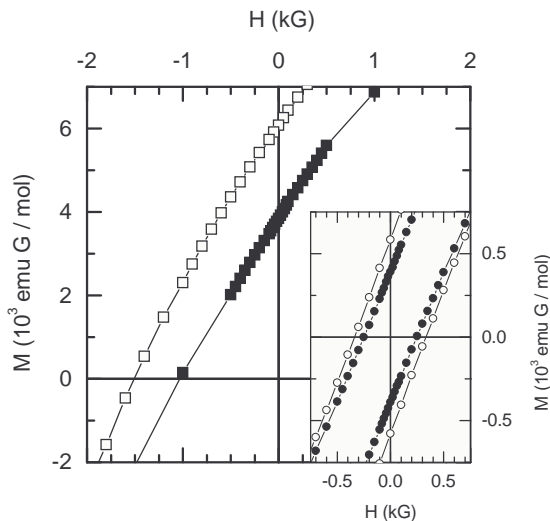


FIG. 5: The $T = 2$ K magnetization versus magnetic field sweeps for the two largest sizes of nanoparticles, Batches C and D. The response of Batch D is symmetric, so only the upper branches of the hysteresis curves are shown for the light (\square) and dark (\blacksquare) states. The inset shows the hysteresis loops for Batch C in the light (\circ) and dark (\bullet) states. The coercive fields, H_c , for the light and dark states for each batch are listed in Table 1, and the lines are guides for the eyes.

the largest sets of particles but not for the smallest set of particles, Fig. 5 and Table 1.

In conclusion, we have synthesized four different sizes of $\text{Rb}_j\text{Co}_k[\text{Fe}(\text{CN})_6]_l \cdot n\text{H}_2\text{O}$ nanoparticles protected by PVP. Each batch of particles is photoinducible, but the strength of this effect, as well as other global properties, e.g. T_c and H_c , are correlated with the intrinsic particle size distributions of each batch. The combination of photoinduced magnetism and nanosized Prussian blue analog particles with finite coercive fields is unique and establishes a length scale limit of ~ 10 nm for these properties. The next advances in the field will undoubtedly employ Prussian blue analogs with higher transition temperatures [39] that may have a variety of technical applications, including, for example, the exploitation of optically controlled magnetocaloric properties [40].

This work was supported, in part, by NSF DMR-0305371 (MWM) and NSF DMR-0543362 (DRT). We acknowledge early contributions by N. E. Anderson, J. Long, and J.-H. Park. We thank the UF Department of Geology for the ICP-MS work and the UF Major Analytical Instrumentation Center for the TEM images.

[1] K. R. Dunbar and R. A. Heintz, in *Progress in Inorganic Chemistry*, edited by K. D. Karlin (Wiley and Sons, New York, 1997), Vol. 45, p. 283.

- [2] M. Verdaguer and G. Girolami, in *Magnetism: Molecules to Materials V*, edited by J. S. Miller and M. Drillon (Wiley-VCH, Weinheim, 2004), p. 284.
- [3] D. Davidson and L. A. Welo, *J. Phys. Chem.* **32**, 1191 (1928).
- [4] A. N. Holden *et al.*, *Phys. Rev.* **102**, 1463 (1956).
- [5] R. M. Bozorth, H. J. Williams, and D. E. Walsh, *Phys. Rev.* **103**, 572 (1956).
- [6] A. Ito, M. Suenaga, and K. Ôno, *J. Chem. Phys.* **48**, 3597 (1968).
- [7] H. J. Buser *et al.*, *Inorg. Chem.* **16**, 2704 (1977).
- [8] P. Day *et al.*, *Helv. Chim. Acta* **63**, 148 (1980).
- [9] O. Sato *et al.*, *Science* **272**, 704 (1996).
- [10] S. Ohkoshi and K. Hashimoto, *J. Photochem. and Photobiol. C: Photochem. Rev.* **2**, 71 (2001).
- [11] F. Varret, M. Nogues, and A. Goujon, in *Magnetism: Molecules to Materials I*, edited by J. S. Miller and M. Drillon (Wiley-VCH, Weinheim, 2002), p. 257.
- [12] T. Yamamoto *et al.*, *Chem. Lett.* **33**, 500 (2004).
- [13] J.-H. Park *et al.*, *Appl. Phys. Lett.* **85**, 3797 (2004).
- [14] T. Yamamoto *et al.*, *Chem. Mater.* **16**, 1195 (2004).
- [15] J.-H. Park *et al.*, *Polyhedron* **24**, 2355 (2005).
- [16] T. Yamamoto *et al.*, *J. Am. Chem. Soc.* **127**, 16065 (2005).
- [17] J.-H. Park, Ph.D. thesis, University of Florida, 2006 (unpublished).
- [18] F. A. Frye *et al.*, *Polyhedron*, to be published.
- [19] J. G. Moore *et al.*, *Angew. Chem.* **115**, 2847 (2003).
- [20] L. Catala *et al.*, *Chem. Commun.* 746 (2005).
- [21] T. Uemura, and S. Kitagawa, *J. Am. Chem. Soc.* **125**, 7814 (2003).
- [22] T. Uemura, M. Ohba, and S. Kitagawa, *Inorg. Chem.* **43**, 7339 (2004).
- [23] F. A. Frye *et al.*, *Polyhedron*, to be published.
- [24] ImageJ. <http://rsb.info.nih.gov/ij/>.
- [25] Similar size distributions have been obtained for Prussian blue nanoparticles protected by PVP, see Yu. Xian *et al.*, *Anal. Chim. Acta* **546**, 139 (2005).
- [26] K. Yoshizawa *et al.*, *Phys. Chem. B* **102**, 5432 (1998).
- [27] T. Kawamoto, Y. Asai, and S. Abe, *Phys. Rev. Lett.* **86**, 348 (2001).
- [28] A. Bleuzen *et al.*, *J. Am. Chem. Soc.* **122**, 6648 (2000).
- [29] C. Cartier dit Moulin *et al.*, *J. Am. Chem. Soc.* **122**, 6653 (2000).
- [30] V. Escax *et al.*, *J. Am. Chem. Soc.* **123**, 12536 (2001).
- [31] G. Champion *et al.*, *J. Am. Chem. Soc.* **123**, 12544 (2001).
- [32] N. Shimamoto *et al.*, *Inorg. Chem.* **41**, 678 (2002).
- [33] V. Escax *et al.*, *Angew. Chem. Int. Ed.* **44**, 4798 (2005).
- [34] The frequency (1 Hz – 1 kHz) dependences of the peaks in the ac susceptibilities of the ZFC dark states of Batches C and D are consistent with the presence of larger domains of primordial high-spin regions in the largest particles, and these results will be reported elsewhere.
- [35] M. Hanawa *et al.*, *J. Phys. Soc. Jpn.* **72**, 987 (2003).
- [36] Z. Salman *et al.*, *Phys. Rev. B* **73**, 174427 (2006).
- [37] J. A. Mydosh, *Spin Glasses: An Experimental Introduction* (Taylor and Francis, London, 1993).
- [38] D. A. Pejaković *et al.*, *Phys. Rev. Lett.* **85**, 1994 (2000).
- [39] E. Ruiz *et al.*, *Chem. Eur. J.* **11**, 2135 (2005).
- [40] E. Manuel *et al.*, *Phys. Rev. B* **73**, 172406 (2006).